J Mater Sci (2009) 44:323–327
DOI 10.1007/s10853-008-2898-1

Seed-assisted sol–gel synthesis and characterization of nanoparticular V_2O_5/anatase

Andreas J. Kruse · Steffen B. Kristensen · Anders Riisager · Søren B. Rasmussen · Rasmus Fehrmann

Received: 27 May 2008 / Accepted: 22 July 2008 / Published online: 5 December 2008

Abstract Nanoparticular supported vanadia materials with crystalline anatase support with a narrow size distribution around 12 nm have been synthesized by a new facile sol–gel, co-precipitation method using decomposable ammonium chloride seed crystals. The materials have been characterized by means of X-ray powder diffraction, transmission electron microscopy and nitrogen physisorption. The synthesized high-surface area anatase particles allowed a loading of up to 15 wt.% vanadia without exceeding monolayer coverage of V_2O_5 in contrast to typical analogous industrial catalysts which only can accommodate 3–5 wt.% vanadia. These materials are promising candidates for improved catalysts for, e.g., oxidation reactions and selective catalytic reduction of NO_X in flue gases.

Introduction

Vanadium oxides on inorganic support materials constitute the most important supported metal oxide catalysts in both heterogeneous and homogeneous industrial applications [1]. In these catalysts, the amount of active vanadium species exposed to the reactants vary with the type of support (typically SiO_2, Al_2O_3, ZrO_2, and TiO_2) and the loading of vanadium oxide on the carrier [2]. Here both the surface area and the oxide type (i.e., textural and surface properties) dictate the maximum amount that can be loaded before surpassing the monolayer coverage leading to crystalline V_2O_5 formation [3]. The prefered choice of support usually depends on the reactive environment of the catalyst during operation as well as the particular reaction in focus. Thus, it is well known that TiO_2, especially in the anatase form, is an excellent support for vanadium oxides making highly active materials for the selective catalytic reduction (SCR) of nitrogen oxides (i.e. deNO_X) by injection of ammonia in power plant flue-gases and other industrial off-gases [4]. The activity of the industrial VO_X/TiO_2-based SCR catalyst is limited by the surface area of the anatase carrier, since only up to one monolayer of the vanadium oxide species can be accepted corresponding to a vanadia loading of 3–5 wt.%. Increased loading results in decreased deNO_X activity and increased ability to oxidize NH_3 and possibly also SO_2 in the flue gas [5]. One approach to improve the efficiency of catalytic materials is to prepare them as nano-sized particles (mean diameter, <100 nm), which in many reactions have shown to be far more reactive than bulk materials [6]. Hence, it is very likely that small catalyst particles of VO_X/TiO_2 will be able to reduce NO_X with increased efficiency to comply with the demand for sufficiently activity during prolonged operation.

In this study, nano-sized particular vanadium oxide/anatase catalysts with vanadia loadings up to 25 wt.% and relatively high-surface areas are synthesized by a sol–gel, co-precipitation procedure involving concomitant hydrolysis of titanium(IV) and vanadium(V) alkoxides in presence of ammonium chloride seed crystals. The materials are further characterized by X-ray powder diffraction

A. J. Kruse · S. B. Kristensen · A. Riisager · R. Fehrmann (✉)
Department of Chemistry and Center for Sustainable and Green Chemistry, Technical University of Denmark, Building 207, 2800 Kgs. Lyngby, Denmark
e-mail: rf@kemi.dtu.dk

S. B. Rasmussen
Instituto de Catálisis y Petroleoquimica (ICP), Consejo Superior de Investigaciones Cientificas (CSIC), Marie Curie 2, Campus de UAM, 28020 Madrid, Spain

(XRPD), transmission electron microscopy (TEM), and nitrogen adsorption. To the best of our knowledge, this is the first report in the literature of sol–gel preparation of nano-sized metal oxide/TiO_2 using seed crystallization, while metal/TiO_2 catalyst materials have been synthesized previously, e.g. Pt/TiO_2 catalysts [7]. Analogous VO_X/TiO_2 materials have also earlier been prepared by hydrothermal methods [8, 9], mechanical blending [10], and flame synthesis [11, 12], and the latter evaluated for SCR deNO_X.

Experimental

Preparation of VO_X/anatase materials

Nano-sized particular vanadium oxide/anatase materials having a V_2O_5 content of 0–25 wt.% were obtained by calcination of materials prepared by a modified new sol–gel procedure [13, 14] involving concomitant hydrolysis of titanium(IV) isopropoxide (97%, Lancaster) and vanadium(V) oxytriethoxide (95%, Aldrich) in acidic ethanol solution in presence of ammonium chloride (≥99.5%, Fluka) as crystallization germ.

In a typical preparation (here exemplified for a material containing 5.2 wt.% V_2O_5), a solution of 1.40 g NH_4Cl (26.2 mmol) in 4 mL deionized water was added dropwise to a stirred, ice-cooled solution of 3.70 g Ti(i-C_3H_7O)$_4$ (13.0 mmol), 0.72 g $VO(C_2H_5O)_3$ (0.63 mmol), and 2.43 g glacial acetic acid (40.5 mmol) in 10 mL abs. ethanol. After addition of the aqueous solution, a yellowish gel was formed, which subsequently was aged 20 h under stirring before ethanol, liberated propanol, acetic acid, and excess water were removed under reduced pressure (0.2 mbar, 70–100 °C). Finally, the material was calcined (400 °C, 6 h) in an air stream (300 mL min^{-1}) to decompose the ammonium chloride template and convert the amorphous titania support into crystalline anatase.

Characterization of VO_X/anatase materials

XRPDs of the prepared materials were recorded using Cu-Kα radiation ($\lambda = 1.54056$ nm) in the 2θ interval 5–100° with a Huber G670 Guinier camera.

TEM was performed on a JEM 2000FX apparatus with an accelerating voltage of 300 kV. A suspension of about 2 mg of the powdered samples in 2 mL ethanol was sonicated for 1 h and allowed to settle for 15 min, before a drop was distributed on a 300-mesh copper grid coated with a carbon film with holes.

Nitrogen sorption data were obtained at liquid nitrogen temperature by using a Micromeritics ASAP 2020 apparatus. Before determination of nitrogen adsorption–desorption isotherms, the samples (ca. 0.4 g) were outgassed for 2 h at 200 °C under vacuum. The apparent specific surface areas (S_{BET}) were evaluated by two-parameter linear BET plots in the range $p/p_0 = 0.065$–0.2. The external areas (S_{ext}) were determined with the t-plot method [15, 16]. Due to percolation effects on the desorption branches [17] mesopore size distributions were obtained using data from the adsorption branches by assuming open nonintersecting cylindrical pores [18]. The thickness of the adsorbed layer at each relative pressure was obtained from the classical equation of Harkins and Jura.

Results and discussion

XRPD analysis of the prepared vanadia-titania materials after calcination at 400 °C revealed only crystalline anatase support phase with no peaks originating from residual ammonium chloride template or crystalline V_2O_5 (Fig. 1). This also included the materials with high vanadia loadings ≥15 wt.% corresponding to more than a monolayer (see Table 1), thus indicating a high dispersion of an amorphous vanadia phase as typically found for oxide supported vanadia catalysts [15] due to the relatively low V_2O_5 Tammann temperature ($T_m = 209$ °C). Likewise, broadening of the peaks indicated presence of relatively small anatase particles. Notable, however, less intensive peaks (e.g., at $2\theta = 28$, 33, 43, 45, and 58°), possibly originating from an undisclosed mixed crystalline vanadia-titania phase, were observed for the materials with high vanadia loading. Vanadium cation promoted formation of $V_xTi_{1-x}O_2$ phases

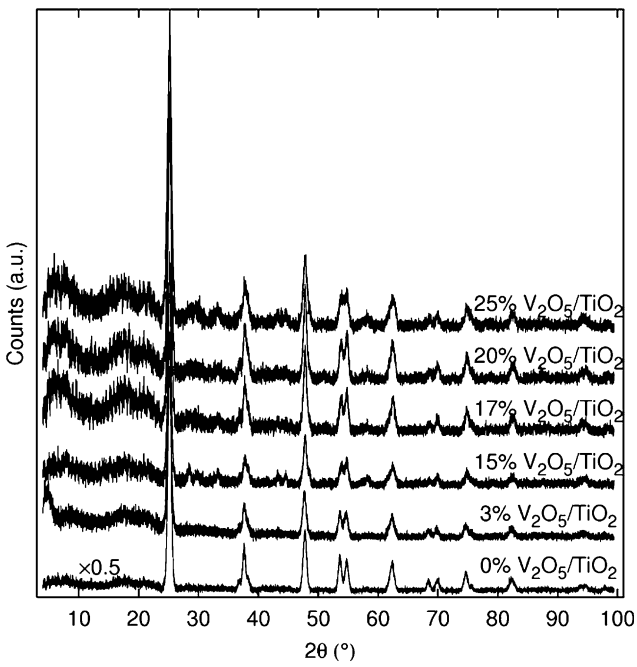

Fig. 1 XRPDs of crystalline VO_X/anatase materials

Table 1 Characteristics of VO_X/anatase materials

V_2O_5 (wt.%)	S_{BET} ($m^2\ g^{-1}$)	S_{ext} ($m^2\ g^{-1}$)	$d_{particle}$ (nm)		n_s[c] (V atoms nm^{-2})
			BET[a]	XRPD[b]	
0.0	73	–	21.1	15.0	–
3.0	108	106	14.2	14.4	1.8
5.2	64	57	24.2	15.8	5.4
7.0	75	65	20.7	17.8	6.2
11	95	91	16.4	15.4	8.2
15	127	127	12.4	15.6	7.7
20	110	106	14.4	15.2	12.0
25	126	121	12.7	11.3	13.3

[a] Crystallite sizes calculated as $d = 6 \cdot ((X_{TiO_2} \cdot \rho_{TiO_2} + X_{V_2O_5} \cdot \rho_{V_2O_5}) \cdot S_{BET})^{-1}$ with $\rho_{V_2O_5} = 3350\,kg\,m^{-3}$ and $\rho_{TiO_2} = 3900\,kg\,m^{-3}$ assuming spherical particle shape [21]

[b] Crystallite sizes calculated by Scherrer's equation as $\Phi = K \cdot \lambda \cdot (B_d \cdot \cos\theta)^{-1}$ with $\lambda_{CuK\alpha} = 1.54056$ nm, the peak form factor $K = 0.9$, the peak width at half hight B_d, and angle ($2\theta = 25.3°$) of the peak corresponding to the (101) reflections

[c] Surface density of vanadium atoms calculated as $n_s = m_{V_2O_5} \cdot 2 \cdot N_A\,(m_{total} \cdot M_{V_2O_5} \cdot S_{BET} \cdot 10^{18})^{-1}$ [22]

incorporating rutile has previously [19, 20] been observed when vanadia-anatase materials were heated to temperatures higher than 500 °C. Also vanadium/titanate composite nanorods have been reported [8] to form under hydrothermal conditions. Further studies towards identifying the minor crystalline phase and its possible effect on catalytic activity in, e.g. SCR of NO_X, are in progress.

The size of the formed oxide crystallites was calculated by Scherrer's equation (using the peak angle $2\theta = 25.3°$) to be in the range of 11–18 nm (see Table 1) with no obvious correlation to the vanadia content. Sequential measurements of the samples during calcination further revealed that anatase crystallization was initiated around 300 °C followed by crystal growth until the particles reached the equilibrium size after 1–2 h.

TEM images of the materials confirmed the high degree of crystallinity of the anatase support and average particle sizes of about 10 nm, as exemplified in Fig. 2 for pure anatase, 7 and 25 wt.% samples. Additionally, the (101) lattice plan of anatase with a distance of 0.35 nm between the atomic layers was clearly identified [23]. In the vanadia-containing samples, an amorphous layer surrounding the nano-sized anatase crystallites with no distinctive structure and a thickness around ca. 0.5 nm could further be attributed to vanadia, while indication of V_2O_5 crystallite formation only became apparent in the 25 wt.% sample (Fig. 2c).

Crystallite sizes comparable to those measured by TEM were also deducted from the measured S_{BET} areas of the materials assuming a spherical shape of particles (see Table 1), thus indicating no significant intra particulate crystal porosity. However, in contrast to the particle size dependency established from the XRPD measurements, a clear tendency towards decreasing crystallite size with increasing vanadia loading was observed from the specific surface area calculations, suggesting significant differences in the texture of the mixed materials depending on the oxide composition.

The pore size distributions of the materials were calculated from nitrogen physisorption isotherms to be relatively well defined with pore diameters in the range of 3–5 nm, increasing with the vanadium loading. Representative size distribution plots are shown for the 3 and 20 wt.% materials in Fig. 3.

For the material with 20 wt.% vanadia loading a shoulder appeared, however, at 8–9 nm suggesting a slightly bimodal pore structure for the catalysts with high loadings of vanadium. For comparison, the pore size distribution of a conventional TiO_2 sample exposed to similar thermal treatment is also shown in Fig. 3. An obvious shift in pore size distribution towards smaller pores is obtained by the new seed-assisted sol–gel method. Thus, the new

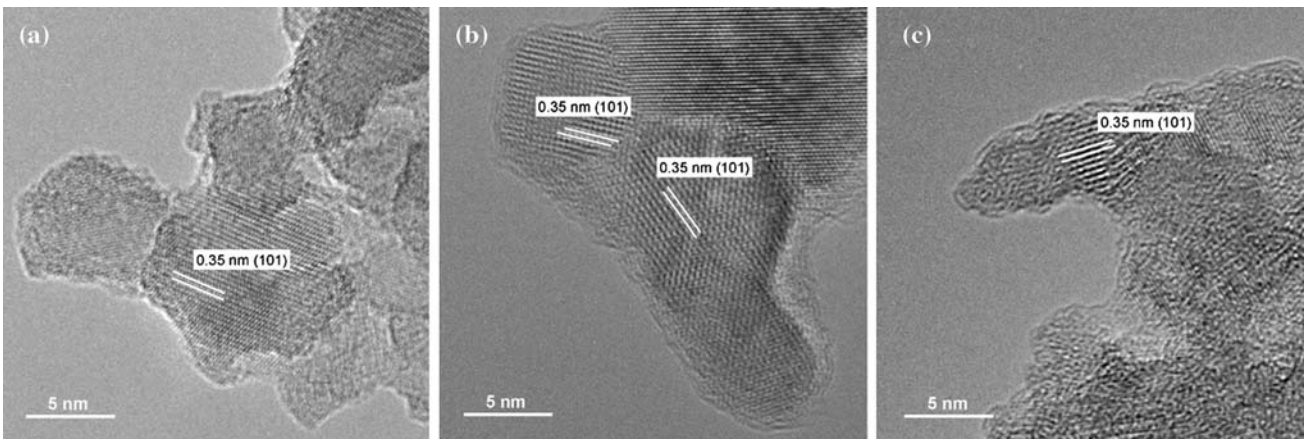

Fig. 2 TEM micrographs of prepared (**a**) anatase, (**b**) 7 wt.% VO_X/anatase and (**c**) 25 wt.% VO_X/anatase materials

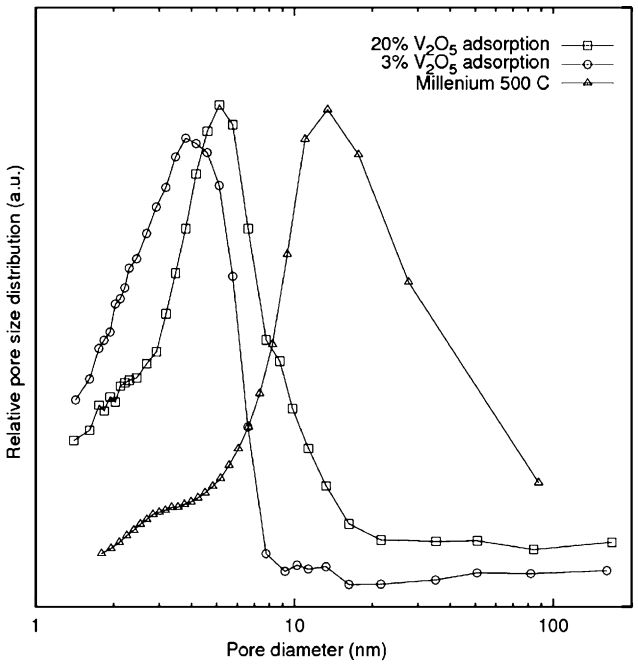

Fig. 3 Pore size distributions obtained from nitrogen sorption data for 3 and 20 wt.% VO_X/anatase materials and a commercial pure anatase support (TIONA-G5, Millennium Co.), respectively

materials have a pore structure which can be characterized as being between micro- and meso-pores. Microporosity as such is not desirable for catalyst materials, due to possible diffusion limitations to the less accessible surface. However, calculations of the external surface areas by the *t*-plot method yielded values virtually identical to those derived from the BET equation (see Table 1). This confirmed that essentially all surface area originated from none microporous structures, yielding readily accesible surface vanadia species for gas-phase molecules. The observed increase in pore sizes combined with the increased areas is not observed for vanadia/TiO_2 materials synthesized by conventional impregnation methods. Here a decrease is usually observed along with the filling of the pore system [24]. The phenomenon observed here can be explained by the induced added distance between the anatase particles by the vanadium salt during the co-precipitation step. After calcination, the precursor transforms to mobile oxo-vanadium species, which disperse over the high-surface area of TiO_2, leaving the framework with increased porosity, wider pores and added surface roughness.

Conclusions

Nano-particle VO_X/TiO_2 materials have for the first time been prepared by co-precipitation of vanadia and titania by a seed-assisted sol–gel, co-precipitation method. The calcined material consisted of crystalline anatase particles covered with amorphous vanadia with a very uniform size distribution of around 12 nm. The small particle size of the anatase support (due to the corresponding high-surface area) allowed high loading of up to 15 wt.% vanadia without exceeding monolayer coverage of V_2O_5 in contrast to typical industrial catalysts which only can accommodate 3–5 wt.%.

Recently, comprehensive studies of the activity of these nano-VO_X/TiO_2 catalysts for both oxidation reactions and SCR of NO_X in flue-gases by NH_3 have been initiated. Preliminary results here indicate a superior activity compared to traditional catalysts, thus suggesting that the nano-materials might prove useful where small catalyst bed volumes or SCR catalysts with prolonged life on steam are desired. This is especially the case for biomass-fired power plants (or co-fired with fossil fuels), where the aggressive K-containing flue-gas rapidly decreases the activty of the traditional deNO_X catalysts [25–28].

Acknowledgements The Center for Sustainable and Green Chemistry is sponsored by the Danish National Research Foundation, and the work was supported by the Danish Research Council for Technology and Production Sciences, Elkraft Systems (PSO FU5201), the USACH Program and the Communidad Autónoma de Madrid (CAM-GR/AMB/0751/2004). We thank K. Egeblad and S.K. Klitgaard (Technical University of Denmark) for the TEM recordings.

References

1. Weckhuysen BM, Van Der Voort P, Catana G (eds) (2000) Spetroscopy of transition metal ions on surfaces. Leuven University Press, Leuven
2. Gao X, Wachs IE (2002) Top Catal 18:243. doi:10.1023/A:1013842722877
3. Weckhuysen BM, Keller DE (2003) Catal Today 78:25. doi:10.1016/S0920-5861(02)00323-1
4. Parvulescu VI, Grange P, Delmon B (1998) Catal Today 46:233. doi:10.1016/S0920-5861(98)00399-X
5. Busca G, Lietti L, Ramis G, Berti F (1998) Appl Catal 18:1. doi:10.1016/S0926-3373(98)00040-X
6. Astruc D, Lu F, Aranzaes JR (2005) Angew Chem Int Ed 44:7852. doi:10.1002/anie.200500766
7. Wang X, Landau MV, Rotter H, Vradman L, Wolfson A, Erenburg A (2004) J Catal 222:565. doi:10.1016/j.jcat.2003.12.003
8. Yu L, Zhang X (2004) Mater Chem Phys 87:168. doi:10.1016/j.matchemphys.2004.05.022
9. Mohamed MM, Bayoumy WA, Khairy M, Mousa MA (2006) Microporous Mesoporous Mater 97:66. doi:10.1016/j.micromeso.2006.07.028
10. Liu G, Wang K, Zhou Z (2006) Mater Sci Forum 510–511:86
11. Stark WJ, Wegner K, Pratsinis SE, Baiker A (2001) J Catal 197:182. doi:10.1006/jcat.2000.3073
12. Schimmoeller B, Schulz H, Pratsinis SE, Bareiss A, Reitzmann A, Kraushaar-Czarnetzki B (2006) J Catal 243:82. doi:10.1016/j.jcat.2006.07.007
13. Hari-Bala, Zhao J, Jiang Y, Ding X, Tian Y, Yu K, Wang Z (2005) Mater Lett 59:1937

14. Hari-Bala, Guo Y, Zhao X, Zhao J, Fu W, Ding X, Jiang Y, Yu K, Lv X, Wang Z (2006) Mater Lett 60:494 doi:10.1016/j.matlet.2005.09.030
15. Lippens BC, de Boer JH (1965) J Catal 4:319. doi:10.1016/0021-9517(65)90307-6
16. Rouquerol F, Rouquerol J, Sing K (1999) Adsorption by powders and porous solids—principles, methodology and applications. Academic Press, London
17. Groen JC, Pérez-Ramírez J (2004) Appl Catal A 268:121. doi:10.1016/j.apcata.2004.03.031
18. Mellqvist J, Rosén A (1996) J Quant Spectrosc Radiat Transfer 56:87
19. Hausinger G, Schmelz H, Knözinger H (1988) Appl Catal 39:267. doi:10.1016/S0166-9834(00)80954-9
20. Grzybowska-Świerkosz B (1997) Appl Catal A 157:263. doi:10.1016/S0926-860X(97)00015-X
21. Lide DR (ed) (2007) CRC handbook of chemistry and physics, 87th edn. Taylor and Francis, Boca Raton, FL
22. Kamata H, Takahashi K, Odenbrand CUI (1999) J Mol Catal A 139:189. doi:10.1016/S1381-1169(98)00177-0
23. Dmitri A, Kiwi-Minsker L, Zaikovskii V, Renken A (2000) J Catal 193:145. doi:10.1006/jcat.2000.2872
24. Yates M, Martín JA, Martín-Luengo JA, Suarez S, Blanco J (2005) Catal Today 107–108:120. doi:10.1016/j.cattod.2005.07.015
25. Kustov AL, Kustova MY, Fehrmann R, Simonsen P (2005) Appl Catal B 58:97. doi:10.1016/j.apcatb.2004.11.016
26. Zheng Y, Jensen AD, Johnsson JE (2005) Appl Catal B 60:253. doi:10.1016/j.apcatb.2005.03.010
27. Due-Hansen J, Kustov AL, Rasmussen SB, Fehrmann R, Christensen CH (2006) Appl Catal B 66:161. doi:10.1016/j.apcatb.2006.03.006
28. Due-Hansen J, Boghosian S, Kustov AL, Fristrup P, Tsilomelekis G, Ståhl K et al (2007) J Catal 251:459. doi:10.1016/j.jcat.2007.07.016